Improving Structural Test and Analysis Correlation Using Digital Image Correlation Boundary Measurements

Andrew E. Lovejoy[1]
NASA Langley Research Center, Hampton, VA 23681, United States of America

Nathaniel W. Gardner[2] and David S. Dawicke[3]
Analytical Services and Materials, Inc., Hampton, VA 23666, United States of America

Christine V. Jutte[4]
Craig Technologies, Inc., Merritt Island, FL 32953, United States of America

Benjamin Smith[5]
Aurora Flight Sciences, Inc., Beavercreek, OH 45431, United States of America

Simplified idealizations, such as clamped or simply supported, are commonly used as support boundary conditions in modeling and analysis of tested aerospace structures. However, these simplifications are not always appropriate and characterization of the response of non-rigid boundaries is often required to improve test and analysis correlation. While analysis models are typically modified to better represent the test, this modification is often not practical due to the complexities of the boundary response. A study is conducted to examine the use of digital image correlation (DIC) to measure the boundary support structure response and then to adjust the test data to remove the effects of the boundary response in order to improve test and analysis correlation. A high-aspect ratio composite wing test is the subject of the study. Three sources of boundary flexibility contributing to rigid body rotation of the test wing are identified and quantified using both DIC and conventional test data. The wing displacement test data are adjusted using DIC data for these sources. Wing displacement test data is also adjusted using direct measurement of wing rotation from a DIC system that monitored the top surface, root region of the wing, and using available conventional instrumentation. The adjusted data exhibits improved test and analysis correlation and demonstrated the benefit of using DIC along with conventional instrumentation to collect and interpret test data.

I. Nomenclature

$\theta_{x,AP}$ = Rigid body rotation angle of the attachment pins about the global x-axis
$\theta_{x,Inc}$ = Rigid body rotation angle of the wing about the global x-axis, measured by the inclinometer at the root
$\theta_{x,RP}$ = Rigid body rotation angle of the reaction plates about the global x-axis

[1] Research Aerospace Engineer, Structural Mechanics and Concepts Branch, Associate Fellow AIAA.
[2] Digital Image Correlation Specialist.
[3] Senior Scientist.
[4] Principal Engineer.
[5] Research Engineer.

$\theta_{x,RT}$ = Rigid body rotation angle of the reaction table about the global x-axis
$\theta_{x,Wing}$ = Rigid body rotation angle of the wing about the global x-axis
$\theta_{y,AP}$ = Rigid body rotation angle of the attachment pins about the global y-axis
$\theta_{y,Inc}$ = Rigid body rotation angle of the wing about the global y-axis, measured by the inclinometer at the root
$\theta_{y,RP}$ = Rigid body rotation angle of the reaction plates about the global y-axis
$\theta_{y,RT}$ = Rigid body rotation angle of the reaction table about the global y-axis
$\theta_{y,Wing}$ = Rigid body rotation angle of the wing about the global y-axis

II. Introduction

Structural testing is commonly performed on aerospace structures to evaluate structural performance and to validate structural analysis codes and models. Validation of structural analysis codes and models is accomplished through the process of test and analysis correlation, whereby measured and predicted responses are compared for qualitative and quantitative agreement. The support boundary conditions in analyses are commonly modeled using simplified idealizations, such as clamped or simply supported. The idealized clamped boundary condition approximation is commonly used when the supporting structure is assumed to be rigid, and therefore the supporting structure is not included in the analysis model because clamped boundary conditions are applied at the test article and support structure interface location(s). However, if the support structure is not sufficiently rigid to warrant the clamped boundary approximation, or if connections within the fixtures are present that allow relative motion between adjacent parts, then the test response can be significantly influenced by the deformations of the supporting structure. In such a case, the boundary structure should be included in the analysis model until a point where classical boundary condition approximations would be valid (e.g, a "ground" condition). However, there are times when the complexity of the support structure, including difficulty in modeling connection conditions, make such an approach less desirable. As a result, characterization of the response of non-rigid boundaries is desirable to improve test and analysis correlation through adjustment of the test results to remove the influence of the boundary support structure response.

The composite wing studied herein is the passive aeroelastic tailored (PAT) wing. The PAT wing was tested as part of the Advanced Air Transport Technology (AATT) Project at NASA. The AATT Project explores and develops technologies and concepts to support the NASA vision for advanced fixed wing transport aircraft that exhibit revolutionary energy efficiency and environmental compatibility. The PAT wing was tested at the NASA Armstrong Flight Research Center (AFRC) in conjunction with the NASA Langley Research Center (LaRC). The wing was designed by Aurora Flight Sciences at their facility in Dayton, Ohio, and was manufactured at their Columbus, Mississippi facility. The PAT wing was a 27% scale representation of a full-scale high-aspect ratio composite wing that included carbon-fiber tow-steering in the upper and lower covers. The full-scale wing was designed with the goal of improving aerodynamic efficiency while minimizing fuel burn by the University of Michigan using an approach similar to that presented in Ref. [1]. The test article was 39-feet long and consisted of the tow-steered covers with conventional laminates used for the ribs and spars. However, manufacturing defects in the as-built wing required repairs which complicated analytical modeling. A complete description of the defects and repairs is provided in Ref. [2].

Testing of the PAT wing was carried out in the late summer and early fall of 2018 wherein the wing was loaded in a -1g down-bending load condition, a 2.5g up-bending load condition and flexural axis loading. Detailed test and analysis correlation are provided in Refs. [2, 3] using standard approaches. Test results for the PAT wing revealed that the root support structure exhibited deformations during loading of the wing, leading to significant errors in test and analysis correlation of the wing deflection [2, 3]. Evaluation of the support structure deformations, and the influence of these deformations on test and analysis correlation due to introduced rigid-body wing rotations was conducted using digital image correlation (DIC) and conventional instrumentation. In this paper, the use of DIC to measure the boundary support structure response of a composite wing test is examined and used to adjust test data for comparison to predicted results. A description of the PAT Wing and test setup is presented first. The characterization of the boundary response using DIC and conventional instrumentation, and a description of the process to apply DIC-measured responses to test data correction is presented next. Test and analysis correlation of the PAT wing to the developed DIC-based boundary correction approach are then presented with a final discussion of the results.

III. PAT Wing Test Description

The PAT wing test set-up at AFRC is shown in Fig. 1 and the steel wing root support structure is shown in Fig. 2. The wing was mounted to two root reaction plates that were connected to the leading and trailing edge spars using four 3-inch-diameter attachment pins, two in each spar. The root reaction plates were connected to a 6-degree-of-freedom reaction table using angle brackets, with the reaction table supported by load cells at six locations atop a base

pedestal. The pedestal was joined to three steel support I-beams that were connected to the load lines, completing a self-reacting test system. Loading was applied using seven pairs of load lines at seven span-wise locations, designated as 1 through 7 from inboard to wing tip, with one actuator at the leading edge (LE) spar and one at the trailing edge (TE) spar at each spanwise location. The load lines were attached to the test article and support I-beams, except for station 7 at the wing tip that was attached to the test article and floor, for the -1g down-bending load condition and flexural axis loading at individual load lines. For the 2.5g up-bending load condition, the outboard three sets of load locations were connected to the overhead load structure identified in Fig. 1, with the steel overhead load structure connected to the support I-beams. The pairs of wing loads at each outboard station were applied using a single loading actuator for each of the load stations, with the three loading actuators embedded in the overhead load structure. Cables connected the loading actuators to the corresponding pairs of wing load connection points at each of the three spanwise loading locations. The cables were guided by movable pulleys that enabled control of the loading direction at each location. The cables were attached to I-beams that split the load to the two wing connection points in a whiffle tree configuration, with the positioning of each overhead cable connection to the I-beam providing the correct load division between the corresponding two wing connection points.

Instrumentation used during the PAT wing testing included strain gages, displacement transducers (DTs), inclinometers, fiber-optic strain sensor (FOSS) wires, and DIC systems. A total of 412 strain gages (axial and rosette), 17 DTs, 36 inclinometers, and 8 FOSS wires with over 7000 FOSS sensors (axial and virtual rosette) were used. AFRC engineers used two DIC systems on the TE side of the wing to monitor the deflection of the PAT wing using bulls-eye targets applied to the wing, to the test fixtures, and to stationary reference surfaces. LaRC engineers used three DIC systems to characterize boundary conditions and wing root deformations, as identified in Fig. 3. One LaRC DIC system, designated as “Top,” was used to monitor the root portion of the wing upper cover and the top surface of the reaction table, as shown in Fig. 4. The other two LaRC DIC systems were used to monitor the boundary support structure, including the root reaction plates, 3-inch-diameter pins, and the reaction table edges. The system designated as “Side A” monitored the TE surfaces, and the system designated as “Side B” monitored the LE surfaces. The DIC speckle pattern for the TE (Side A) side of the support structure is shown in Fig. 5. A similar pattern was applied to the LE (Side B) side, but without the bullseye markers that were used by the AFRC DIC systems. Additional details of the test set-up, loading, and instrumentation are provided in Ref. [3].

IV. DIC Test Results

The PAT wing was subjected to three loading conditions at various loading percentages. Load conditions were 2.5g up-bending, -1g down-bending, and flexural axis single-point load at the 8 outboard locations [3]. During testing of the PAT wing, measured data indicated flexibility of the boundary support structure that resulted in rigid body motion of the wing. This rigid body motion influenced the test and analysis correlation of the wing deflection measurements, but affected the strain measurements much less as those are invariant with rigid body motion. As a result, deflection correlation between test and analysis did not exhibit the desired degree of agreement, and further investigation was performed to determine if correlation could be improved by taking into account the response of the test boundary support structure. Flexibility of the boundary support structure is examined herein for the 2.5g up-bending condition, as that condition exhibited the greatest wing rigid body motion. Additionally, the results and discussion presented herein focus on the final load sequence for the 2.5g up-bending condition, where there were load holds at 25%, 50%, and 75% of the maximum intended load. However, the maximum loads reached were approximately 90% of the intended maximum loads due to an event that occurred near the LE reaction plate that caused the load control system to exhibit uncontrolled oscillations. Those oscillations necessitated that the load be removed. During the unloading process, several of the load locations were subjected to loads in excess of those intended. As a result, the 100% load level was not obtained, and the wing was not re-tested. The total load as a function of time after midnight is shown in Fig. 6. The horizontal dash/double-dot lines indicate the three load holds and the final maximum load of approximately 90%, and those lines are included in many of the subsequent plots herein to identify those locations. Lastly, while the focus of this study is on the DIC results and how they can be used to improve test and analysis correlation, equivalent conventional instrumentation test data are presented whenever possible to support the DIC data. The remainder of this section presents data that indicate flexibility of the boundary support structure, and possible sources of the observed flexibility are identified and quantified.

Flexibility of the boundary support structure was apparent during testing, and data from multiple locations and instrumentation were used to identify the sources of flexibility. Data that initially indicated flexibility of the boundary structure was the vertical displacement at the LE and TE locations, as measured by the DTs. The measured displacements at the second set of load lines, located at approximately 30% of the span is shown in Fig. 7. A noticeable nonlinear response in the form of a displacement discontinuity occurred in the measurements at about 500 lb of total

load. Another, much smaller, discontinuity in displacement was observed in the measured data at just over 2000 lb of total load. Additionally, the slopes of the test data are less than the predicted results, indicating an apparent reduced stiffness in the test compared to the analysis. The behavior exhibited in Fig. 7 and in the response of other test data suggested the need for a more in-depth examination of the boundary support structure response.

The first potential contributor to the rigid body rotations was the 3-inch attachment pins connecting the reaction plates to the wing spars as shown in Fig. 2. The 3-inch attachment pin total displacements were measured from their initial position within the root reaction plates. The displacements of the 3-inch attachment pins, as measured by the DIC system, exhibited rapid nonlinear response (discontinuities), as shown in Fig. 8. These pin discontinuities are indicators of pin slop, movement of the pin in a loose hole, that could contribute to the observed wing deflection by allowing rigid body rotation of the wing with respect to the root mount plates. These discontinuities in the attachment pin displacements occurred at about 500 lb of load, and thus correspond to the large discontinuities in displacement indicated in Fig. 7 at approximately the same load. This correlation in load suggests that the first source of boundary support structure flexibility was pin slop of the attachment pins in the reaction plates. Based on the results plotted in Fig. 8, it was observed that the discontinuity was essentially a single event, with only the Side B outboard pin showing any significant variation as load was applied after the initial displacement discontinuities. However, for loads greater than about 5000 lb, the displacements are relatively invariant at all pin locations, indicating that the attachment pin displacement discontinuities, or pin slop, represents a single nonlinear event.

Calculated rigid body rotation angles at the 900 lb and 5000 lb load levels are presented in Table 1. Rigid body rotation angles about the global x-axis, $\theta_{x,AP}$ calculated for the pairs of pins on Sides A and B, and the set of rigid body rotation angles about the global y-axis, $\theta_{y,AP}$ calculated for the pairs of pins located inboard (IB) and outboard (OB) are shown in the Table 1. Also included in the table are the average rotation angles about the x- and y-axes. The 5000 lb load is representative of the 3-inch pin displacement response after the discontinuity occurred and during the majority of the loading due to the previously mentioned invariance above that load. The 900 lb load is shown because the majority of the pin displacement continuity occurred prior to that load level. The first observation was that the average rotations about the x-axis at 900 lb (where the large displacements initially settled out) and at 5000 lb are within about 1% of each other, where the 5000 lb load was the basis for the percent error calculations. Second, the average rotations about the y-axis at 900 lb and 5000 lb are within about 45% of each other, with the magnitude of the rotation at 900 lb larger than the magnitude at 5000 lb. However, the rotation about the y-axis is more than an order of magnitude less than that about the x-axis, therefore, the observed relatively large percentage error in the y-axis rotation was deemed less significant. Therefore, in Section V for the test and analysis correlation, the test data corrections using the DIC-calculated rigid body rotations due to reaction plate attachment pin slop for loads above 900 lb use a single rotation set of $\theta_{x,AP} = 0.187°$ and $\theta_{y,AP} = -0.0042°$ that are from the 5000 lb load level. Test data values between 500 lb and 900 lb were ignored in data adjustment as they represent the nonlinear step region that is difficult to quantify, and test data below 500 lb was not corrected to account for the attachment pin slop as it had not yet occurred. It is important to note that no conventional instrumentation measurements were available to compare to these DIC-calculated rotations. Additionally, it would be extremely difficult to obtain the required data through conventional instrumentation since the test set-up would be very complicated in order to measure the two components of in-plane displacement of the pins captured by the DIC.

In addition to the attachment pin slop, the DIC systems designated Side A and Side B measured displacements and deformations of the reaction table edges. A second possible contributor to the wing rigid body rotations was rotation of the reaction table itself. Displacements at the edges of the table were measured for comparison to DTs located between the reaction table and the top of the pedestal in order to monitor rotations of the table. The locations of the DTs relative to the reaction table are shown in part a) of Fig. 9 and the positions from which DIC-measured displacements were taken are shown in part b). In addition to the reaction table rotations calculated from the displacement measurements, an inclinometer was mounted on the top of the reaction table to provide direct measurement of the table rotations. The inclinometer was mounted in the center of the table and was aligned with the wing global axes. The measured displacements from the DTs and DIC are shown in Fig. 10. Both sets of data indicate nonlinear response in the form of displacement discontinuities at load slightly greater than 2000 lb and around 11,800 lb. These displacement discontinuities correspond to pin slop in the load line connections at the outboard reaction table location and the inboard trailing edge reaction table location, respectively, as identified in Fig. 11. The pin slop at these locations occurs at both ends of the links connecting the reaction table to the load cells, and is a consequence of the weight being lifted off the outboard load line as the wing is loaded upward. Then, the twisting of the wing caused the compression load to become a tension load at the inboard trailing edge reaction table load line location. The reaction table rotations, $\theta_{x,RT}$ and $\theta_{y,RT,}$ calculated using DTs, calculated from DIC data, and directly measured by an inclinometer are shown in Fig. 11. Results from all three measurement sources exhibit step changes in angle when the load line pin slop conditions occur 11,800 lb for $\theta_{y,RT}$, and at both 2000 lb and 11,800 lb for $\theta_{x,RT}$.

However, $\theta_{x,RT}$ and $\theta_{y,RT}$ also exhibit continuous rotation angle changes that may be due to the elasticity of the connecting structure, including connection points and the pedestal. All three measurements show excellent agreement in $\theta_{y,RT}$ for load less than 11,800 lb, but the DT values for load greater than 11,800 lb show a different slope than the inclinometer and DIC data. All three measurements show excellent agreement in $\theta_{x,RT}$ for load less than 2000 lb, but the DIC values for load greater than 2000 lb show a different slope than the inclinometer and DT data. However, when used to correct test data in Section V, the values for the reaction table rotations $\theta_{x,RT}$ and $\theta_{y,RT}$ are taken from the DIC data shown in Fig. 12.

In addition to point displacement measurements used to calculate reaction table rigid body rotations, the DIC systems designated Side A and Side B measured the deformation of the reaction table edge. This deformation was determined by extracting a line of data along the length of the edge that included all three translations. The vertical displacement of the reaction table edge measured by the Side A DIC system at 25%, 50%, 75%, and 90% (maximum obtained load) load levels are shown in Fig. 13, and the vertical displacement of the reaction table edge measured by the Side B DIC system at the same load levels are shown in Fig. 14. The plots of the results shown in both figures suggest that the inboard and outboard portions of the reaction plate deflect under load, as indicated by the distinct kinks in the curves outboard of the locations where the point measurements were taken depicted in Fig. 9. These portions of the reaction table are outboard of the stiffening elements, and are also the locations to which the reaction plate connection angles are mounted to the reaction table to transfer load from the reaction plates into the reaction table. Therefore, elastic deformations of the reaction table at these locations results in rigid body motion of the reaction plates and their connection angles. In the current assessment, the reaction plates and their associated connection angles are considered to be rigid, as the reaction plates are subjected to in-plane bending and the connection angles are gusseted. The relative motions of the inboard and outboard portions of the reaction plate were used to calculate rotations of the reaction plate structures. The rotations of the reaction plates about the x-axis, $\theta_{x,RP}$ and the y-axis, $\theta_{y,RP}$ are shown in Table 2. $\theta_{x,RP}$ is the calculated rotation of the reaction plates about the x-axis, and $\theta_{y,RP}$ is the relative rotation of the wing about the y-axis resulting from unequal x-axis rotation of the reaction plates. When used to correct test data in Section V, the values for the reaction plate rotations $\theta_{x,RP}$ and $\theta_{y,RP}$ are taken from Table 2.

In summary, three sources of boundary support structure flexibility have been identified as 1) reaction plate attachment pin slop (discrete step nonlinearity), 2) reaction table load line slop (discrete step nonlinearity) and reaction table elastic deformation (continuous function of load), and 3) reaction plate rotation resulting from reaction table elastic deformation (continuous function of load). The wing total rigid body rotations are a linear combination of the calculated rotations associated with each of these three components. While the reaction table load line slop is discrete, the total combined rotation was provided in Fig. 12 and was used when calculating the total wing rotations. Additionally, while only values at specific load levels were calculated and provided for the reaction plate rotations due to reaction table deformations, it was possible to generate a functional relationship with load to use for data plotted versus load. Therefore, the load-dependent total wing rigid body rotations are defined in two regions as:

$$\begin{aligned} \theta_{x,Wing} &= \theta_{x,RT} + \theta_{x,RP} && , \quad \text{Total Load} < 5000 \text{ lb} \\ &= \theta_{x,AP} + \theta_{x,RT} + \theta_{x,RP} && , \quad \text{Total Load} \geq 5000 \text{ lb} \end{aligned}$$

$$\begin{aligned} \theta_{y,Wing} &= \theta_{y,RT} + \theta_{y,RP} && , \quad \text{Total Load} < 5000 \text{ lb} \\ &= \theta_{y,AP} + \theta_{y,RT} + \theta_{y,RP} && , \quad \text{Total Load} \geq 5000 \text{ lb} \end{aligned}$$

However, as previously mentioned, test data where displacement discontinuities occur are not reliable. Therefore, these data were ignored in adjusted results (i.e., removed) and the gap connected with a linear segment when comparing to data plotted against load to create smooth, continuous curves to compare to the predicted results.

In addition to using the side systems to identify possible sources of boundary support structure flexibility and to calculate their contributions to the wing rigid body rotation, the top system was used to directly calculate wing rigid body rotations. The position for determining the rotations was adjacent to the inclinometer installed on the wing upper cover near the root to provide comparison of the DIC and conventional instrumentation. The top system DIC was only used to calculate the rotations at the hold and final locations, that is, at the 25%, 50%, 75%, and 90% load levels. The wing rigid body rotation data calculated using the top DIC system and the corresponding root inclinometer data is presented in Table 3. In the following section, displacement data are presented to demonstrate the test data adjustment to account for the rigid body motion resulting from the boundary support flexibility.

V. Test and Analysis Correlation

Test and analysis correlation using the raw test data and corrected data are presented. The corrected data consists of three types. The first correction is based on the DIC-identified sources of boundary flexibility that were developed based on DIC measurements from the Side A and Side B systems. Corrections based on this method are termed herein as adjusted DIC component corrections (Adj. DIC Component), as it incorporates the contributions from the component sources to calculate the global wing rigid body rotations and is represented by the equations provided in the previous section. The second correction is based on the global wing rigid body rotations calculated directly using the DIC top system (Adj. DIC Top System). The third correction is based on the global wing rigid body rotations measured directly by the inclinometer mounted to the top of the wing near the root (Adj. Inclinometer). Test displacement data was adjusted by subtracting the predicted wing rigid body rotations from the test $\theta_{x,Wing}$ and $\theta_{y,Wing}$ rigid body rotation angles, and then calculating the displacement at a particular location resulting from application of these rotation angle differences and the original x- and y-locations of the points where the deflections were measured. The calculated displacements resulting from rigid body rotations of the wing were considered to be the error introduced in the test data, and were subtracted from the measured values to create the adjusted test displacement values.

The first set of test results presented to demonstrate DIC-based adjustment for wing rigid body rotation are the load deflection plots at loading station 2 shown in Fig. 2, which is located at about 30% span. The analysis predictions for load versus displacement comparison plotted in Fig. 15 are shown in red, the raw test data are shown in yellow, the DIC-adjusted test data are shown in dark blue, and a simple adjustment method where the data after the attachment pin displacement discontinuity are shifted by the amount of the displacement discontinuity are shown in light blue. Recall that for comparison to the analysis, data associated with the pin slop displacement discontinuity response regions are removed from the data. It is observed that the DIC-adjusted data shows significantly better correlation with the analysis than the raw test data. Also, the DIC-adjusted data exhibits better correlation with the test than simply removing the discontinuities due to the reaction plate attachment pin and reaction table pin slop, designed as Shift in the plot. The Shift curve was created by shifting all data after the displacement discontinuities by a distance equal to each discontinuity to produce a continuous curve without the displacement discontinuities. However, while the correlation is within about 10% at a total wing load of about 15,000 lb, the slope of the DIC-adjusted test data exhibits slightly different character than the analysis. Overall, the test and analysis correlation using DIC-adjusted test data is good, and significantly better compared to the raw test data.

The next set of test data compared are the displacements along the wing at a fixed load. Displacement traces at the leading and trailing edges were examined and found to be similar, so only trailing edge results are presented herein. The trailing edge deflection at the 25% load level results are shown in Fig. 16 and includes DIC-adjusted data using both the component and top system data, as well as the test data corrected using the inclinometer data. The same comparisons for the maximum load, 90% load level, are shown in Fig. 17. The data presented in the figures indicates that the inclinometer and DIC-adjusted data based on the top system exhibit similar improved correlation with the analysis. This improvement is expected as both methods use a direct measure of wing rigid body rotations to generate the adjustments from essentially the same location on the wing. The DIC-adjusted data based on the three components calculated using the Side A and Side B systems resulted in smaller rigid body rotation angles, and therefore less adjustment to the test data, which leads to less improvement in the test and analysis correlation than the other two methods. Recall that the side systems A and B measured the structure from the reaction plate down to the reaction table edges. As a result, the side systems were able to make measurements necessary to calculate reaction table rotations that can include elastic deformation of the structure below the reaction table that includes the load lines, attachment fittings, links, and the pedestal. The side systems also provided measurements necessary for determining the reaction plate attachment pin displacements. However, due to the attachment pins being held in place with brackets on the outside of the reaction plates shown in Fig. 5, it was not possible to get measurements necessary to determine if the pins rotated within the reaction plates and wing spars to become non-normal to the spar web and reaction plate surfaces, off-axis rotation. Off-axis rotation is possible because the pins are in single shear, which generates a moment that causes a nonuniform bearing force through the spar and plate thicknesses that can lead to local bearing failures. Local bearing failures can result in off-axis rotation of the pins so that they are no longer perpendicular to the spar web and reaction plate surfaces. These bearing failures may also only be within the composite, and therefore do not manifest as a rotation of the pin with respect to the attachment plate. Even if there were rotations of the pins with respect to the reaction plates, the bearing failures that lead to this rotation could result in different response in the spars and reaction plates so such a measurement may not be representative of the complete off-axis rotation response. It would be difficult to fully characterize such an off-axis pin rotation from normal to the spar web and reaction plate surfaces even using DIC, but bearing leading to pin rotations could have significantly contributed in the differences between the component angle values and the values measured using the top DIC system. Additionally, the rotation of

the reaction plates was estimated from the deformation of the reaction table edges, and a more accurate measure of the reaction plate rotations should be made by extracting data directly from points on the reaction plates. However, these reaction plate rotation angles are small and are unlikely to be able to account for the complete discrepancy.

Another observation based on the plots in Figs. 16 and 17 is that the correlation is much better inboard than outboard. Plots of the trailing edge inboard deflections for a) 25% load and b) 90% load focusing on the inboard portion are shown in Fig. 18. Correlation is very good for y-locations on the wing out to approximately 250 inches. Note that the 250-inch y-location is between the load locations 4 and 5. Recall that loading locations 1-4 used load lines pushing from below, while loading locations 5-7 use cables pulling on whiffle tree I-beams from above. The orientations of the inner load lines are well known. However, limitations in the overhead space available did not allow the stroke for the overhead cables to pull normal to the wing surface throughout. The pully locations had to be set, which led to the applied loads initially being oriented slightly inboard, then passing through normal to the surface, then becoming oriented slight outboard such that the loading cables pulled more upward than the follower loads used in the analysis. This upward pull may have increased the upward deflection of the outer portion of the wing, especially at higher loads.

To further explain the differences in agreement, note that there is a splice of the leading-edge spar joining the inner composite portion and the outer aluminum portion slightly inboard of the 275-inch y-location. It is possible that the splice could lead to additional local deformations that manifest near the 250-inch location, resulting in additional wing deflection outboard of this location. The strains were examined to determine if unexpected behavior occurred due to the splice. The axial strains on the upper cover near the leading edge at y-locations of about 166 inches, 213 inches, and 267 inches are shown in Fig. 19. The differences between test and analysis at maximum load at these locations are about 10%, 19%, and 12%, and show slightly worse correlation in the vicinity of the possible excessive local deformation. the rosette strains on the leading-edge spar near the axial strain locations of Fig. 19 are shown in Figs. 20-22. The strains at the three locations are of the same order, however, as the rosette gets closer to the splice location, the errors become much larger, particularly for the spanwise strains. Therefore, it is observed that the local response of the wing at about 200 inches to 250 inches, and in the vicinity of the leading-edge spar splice, exhibits worse correlation between test and analysis than at inboard locations. While several possible sources for the discrepancies in the local response have been proposed, they may not be the only ones, and their contributions to the discrepancies have not been quantified. However, it is likely that discrepancies in local response are an important contributor to the outboard displacements being larger than predicted by the analysis, which is independent of the wing rigid body rotations examined using the DIC data. Overall, correcting the measured displacements by the DIC adjustment based on the top system reduced test and analysis correlation errors from around 19% to within 4% on the inboard half of the wing, and reduced errors from over 15% to within 12% on the outboard half of the wing.

VI. Conclusions

A high-aspect ratio tow-steered composite wing was tested at AFRC to demonstrate passive aeroelastic tailoring. Three DIC systems were included in the test instrumentation to monitor the wing upper cover near the root and the boundary support structure on the leading and trailing edges of the root region. The measured wing deflections exceeded the predicted values and discrete discontinuities in displacements occurred while load was applied as a result of apparent rigid body rotations. Several possible sources for these displacement discontinuities were identified by using DIC systems and conventional instrumentation. These sources were pin slop in the reaction plate attachment pins, rotation of the reaction table due to pin slop and elastic deformation of the underlying structure, and rotation of the reaction plates due to deformations of the reaction table. The contributions to the wing rigid body rotation due to each of the three sources were quantified by monitoring the sides of the boundary support structure using DIC systems. Additionally, the rigid body rotation of the wing was calculated directly using measurements from the top DIC system that monitored the upper cover. The measured test deflections were adjusted to account for the rigid body motions in order to compare to the predicted values. Adjustments were made using inclinometer measurements from the root of the wing, the rotations calculated from the top DIC system, and the combination of the component contributions determined using the side DIC systems. Improvements in the test and analysis correlation were demonstrated for point location displacements, as well as for traces of displacement at a fixed load value. The inclinometer and top DIC system rigid body rotations produced essentially the same adjustment, and therefore the same test and analysis correlation improvement. The wing rigid body rotations calculated using the side systems were smaller than the rotations based on the inclinometer and top DIC system, so the correlation improved, but to a lesser amount. However, it was observed that the test and analysis correlation for the inboard portion of the wing was better than for the outboard portion for all three methods. Several possible reasons for this difference in correlation were provided. Strain data was presented to demonstrate that the errors in strain where the displacement correlation is poor increase, and therefore

this difference in correlation could lead to the worse correlation outboard. Therefore, the error on the outboard portion of the wing is not likely to be caused by the wing rigid body rotations.

The importance of boundary deformations on test response have been demonstrated, and in particular, the usefulness of using DIC to monitor these deflections has been demonstrated. It would be very difficult to measure the described reaction plate attachment pin slop using conventional instrumentation. Also, while using the DIC data to determine possible sources of boundary deformation and calculating their individual contributions is very useful, using DIC to provide a direct measure as was done using the top system can help determine if sources of the deformation may not have been identified and measured. Therefore, using DIC to monitor test fixturing is very important and useful tool, especially in cases like the presented PAT wing test where there are multiple contributing factors. DIC also provides the ability to easily monitor more structural responses simultaneously, but having conventional instrumentation with which to compare DIC results provides a measure of confidence. Lastly, there are times when conventional instrumentation can provide the required data with less effort, such as the inclinometer on the wing upper cover that measured the wing rigid body motion directly, but the DIC data provides significantly more data in case the conventional data is insufficient to provide the required test and analysis correlation accuracy.

References

[1] Brooks, T.R., Martins, J.R.R.A., Kennedy, G.J., "High-Fidelity Aerostructural Optimization of Tow-Steered Composite Wings," Journal of Fluids and Structures, Vol. 88, July 2019, pp. 122-147.

[2] Smith, B., Brooks, T. Leader, M., Chin, T.W., Kennedy, G., Martins, J., and Cesnik, C., "Passive Aeroelastic Tailoring Final Report," NASA CR in preparation.

[3] Jutte, C. V., Wieseman, C. D., Stanford, B. K. and Lovejoy, A. E., "Static Loads Testing of the Passive Aeroelastic Tailored Wing," AIAA paper to be presented, SciTech, Orlando, FL, January 6-10, 2020.

Table 1. Reaction plate attachment pin slop rotation angles.

	$\theta_{x,AP}$ (degrees)			$\theta_{y,AP}$ (degrees)		
Load (lb)	**Side A**	**Side B**	**Average**	**Inner**	**Outer**	**Average**
5000	0.2015	0.1722	0.1869	0.01074	-0.01909	-0.004173
900	0.2044	0.1644	0.1844	0.009754	-0.02195	-0.006070
Pct. Diff.	-1%	5%	1%	9%	-15%	-45%

Table 2. Reaction plate rotation angles due to reaction table deformation.

		$\theta_{x,RP}$ (degrees)			$\theta_{y,RP}$ (degrees)
% Load	**Load (lb)**	**Side A**	**Side B**	**Average**	**Average**
25	6,015	-0.02626	0.007162	-0.009549	0.01273
50	12,030	-0.05371	0.01432	-0.01970	0.02626
75	18,044	-0.08117	0.02089	-0.03014	0.04019
90	21,653	-0.1074	0.02686	-0.04029	0.05371

Table 3. Wing rotation angles calculated using top DIC system, and root inclinometer angles.

% Load	Load (lb)	$\theta_{x,Wing}$ (degrees)	$\theta_{y,Wing}$ (degrees)	$\theta_{x,Inc}$ (degrees)	$\theta_{y,Inc}$ (degrees)
25	6,015	0.3698	-0.1058	0.3560	-0.04773
50	12,030	0.4406	-0.1808	0.3771	-0.09013
75	18,044	0.4703	-0.2568	0.4089	-0.1139
90	21,653	0.5239	-0.3497	0.4346	-0.1299

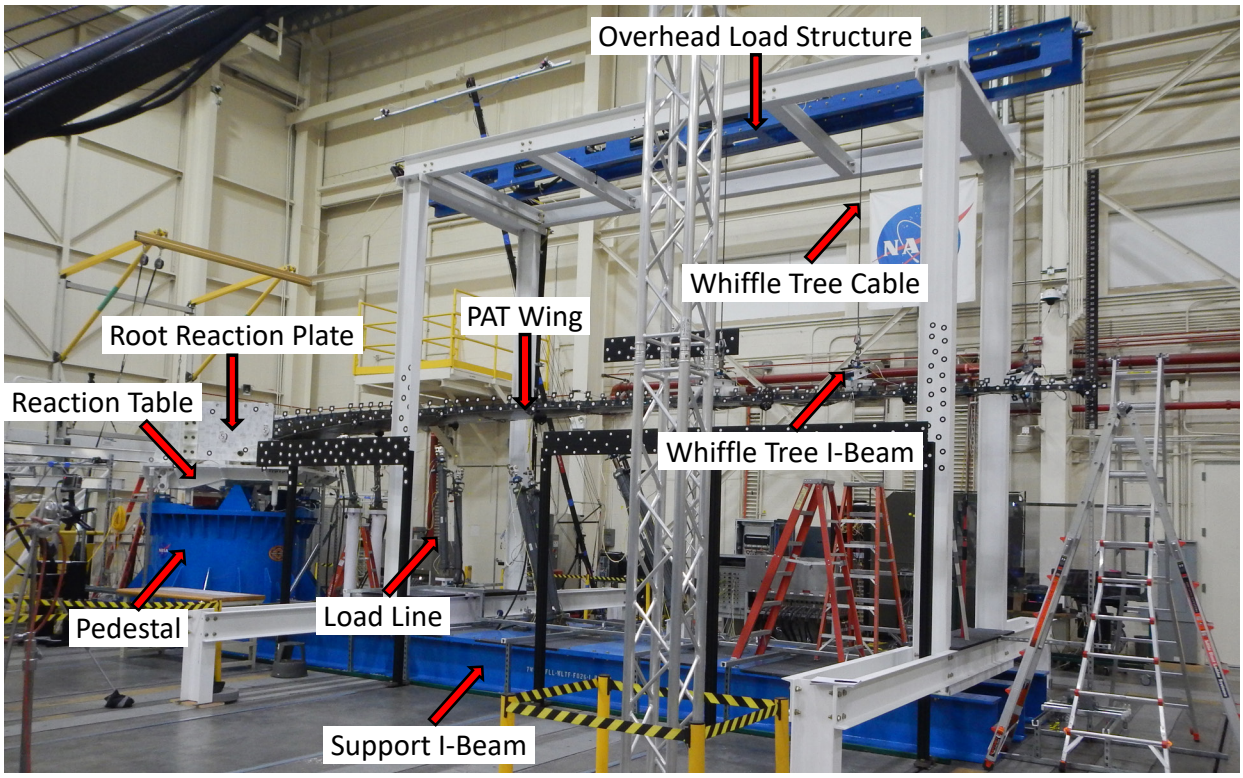

Figure 1. PAT wing test set-up.

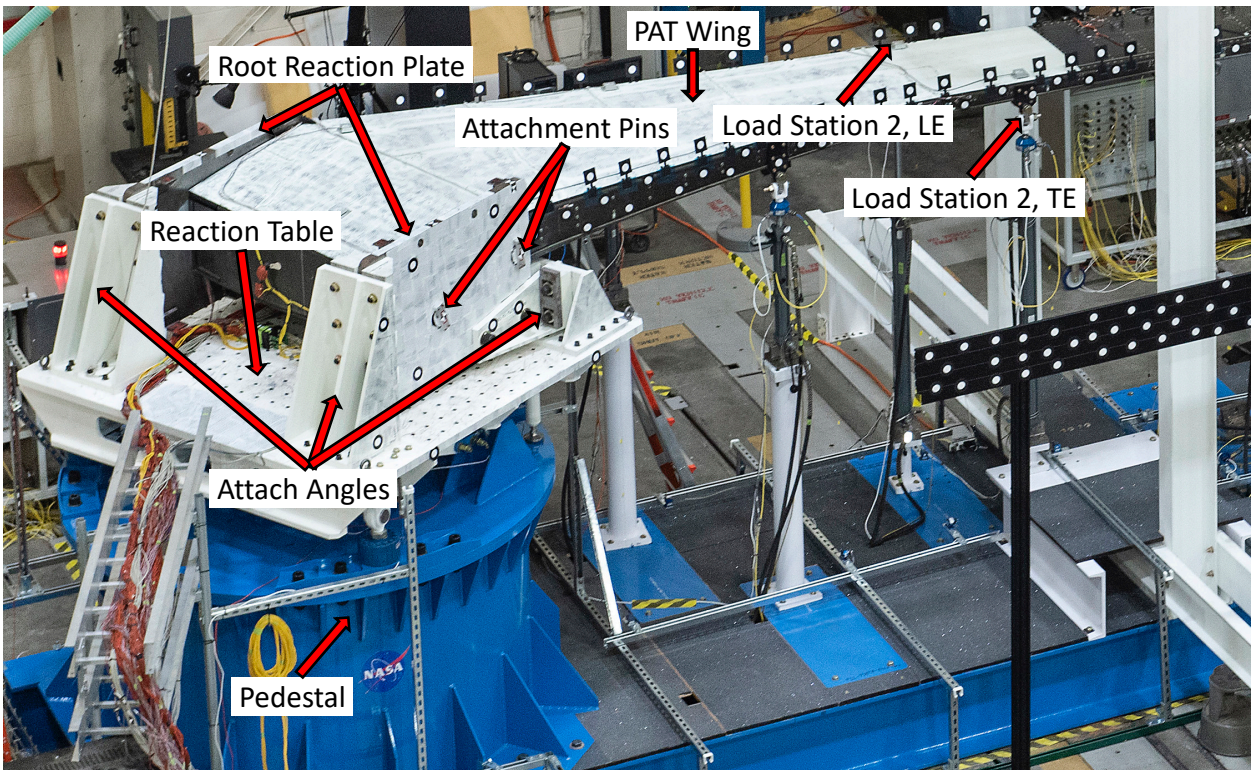

Figure 2. PAT wing root support structure and loading location 2. (Taken from photo AFRC2018-0091-689)

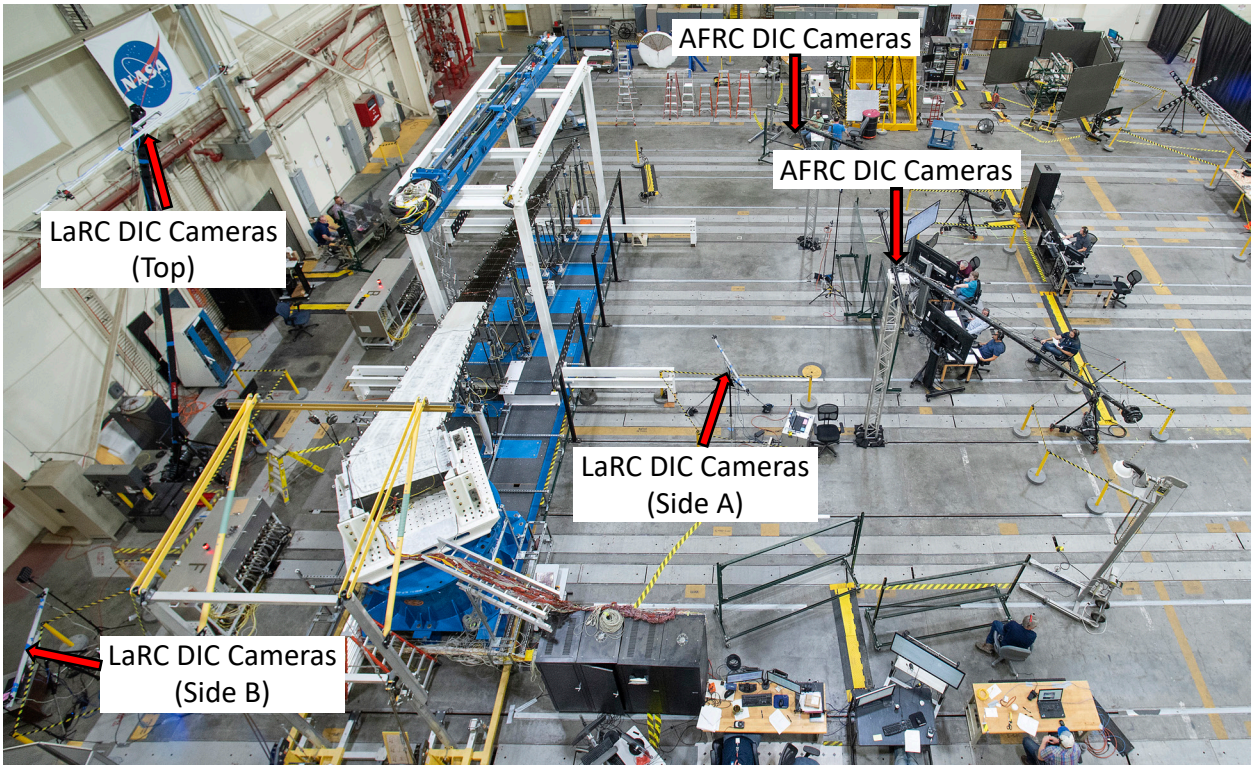

Figure 3. LaRC DIC layout for PAT wing test. (Taken from photo AFRC2018-0091-679)

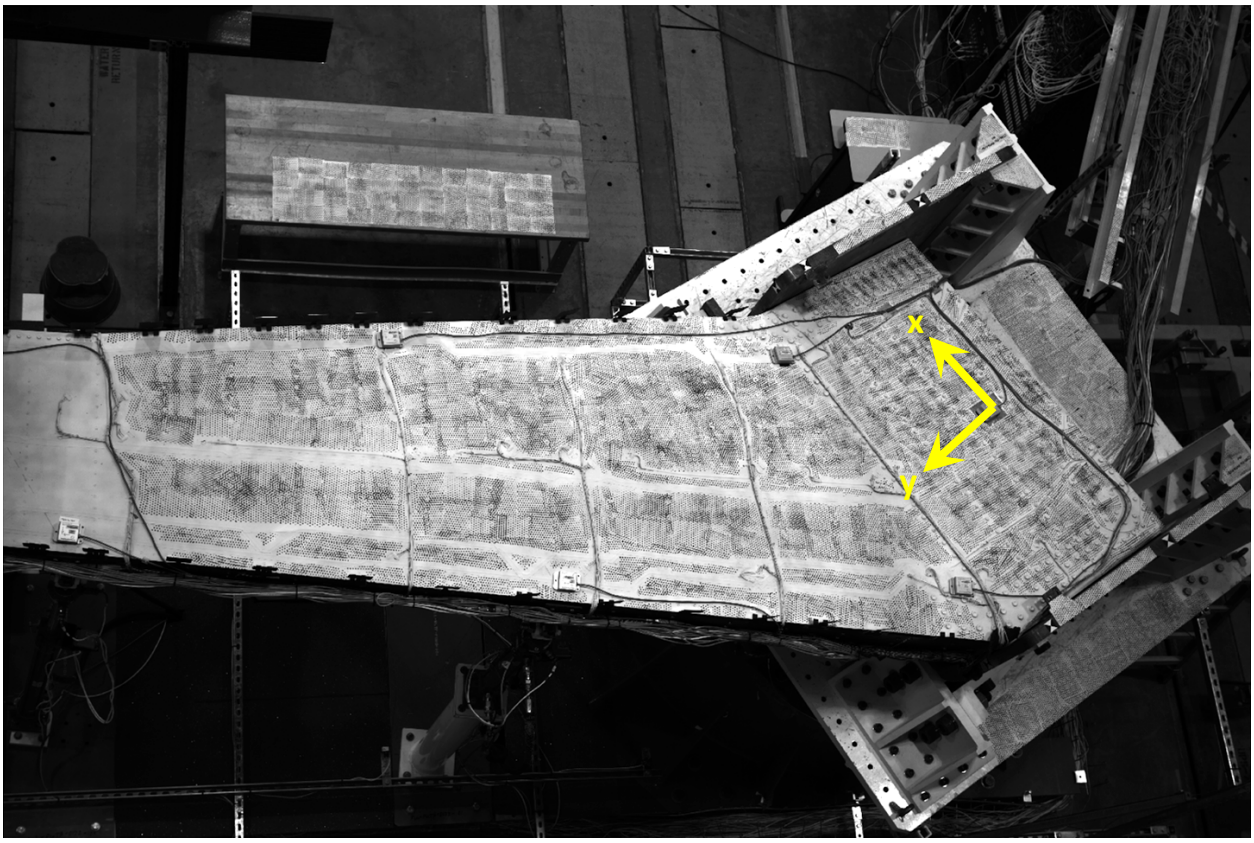

Figure 4. Root upper cover and reaction plate (Top) DIC speckle pattern. Global coordinate system shown.

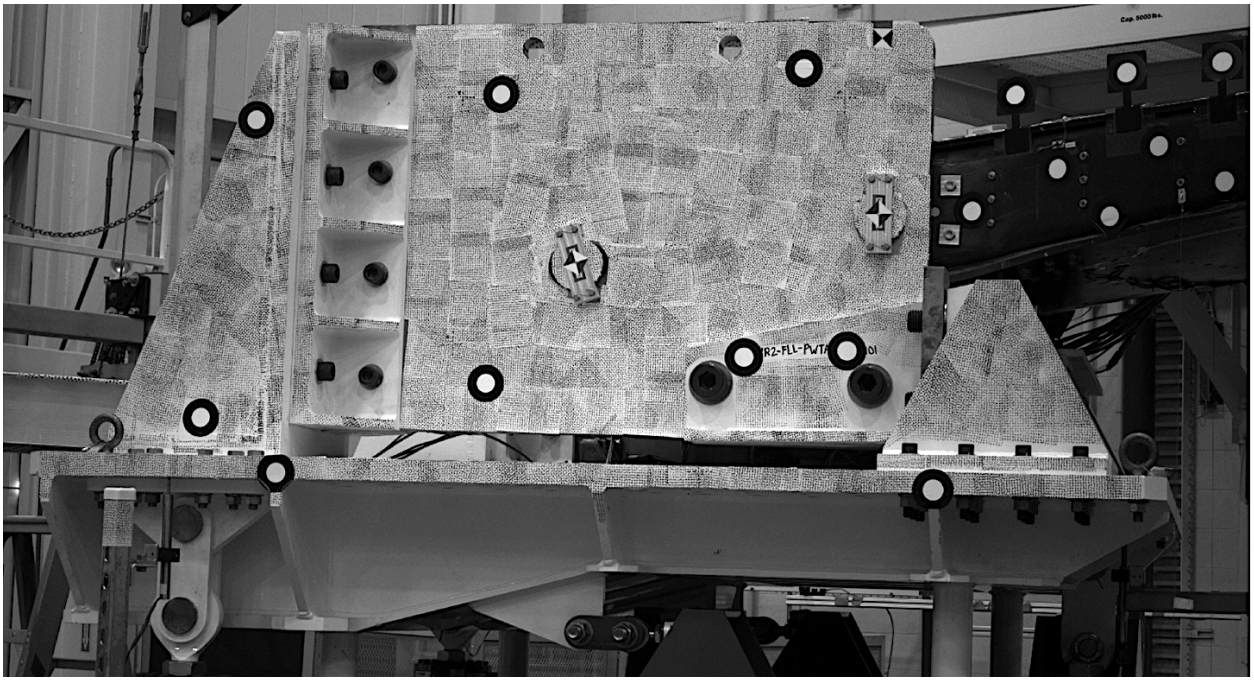

Figure 5. Boundary support structure, trailing edge side (Side A), LaRC DIC speckle pattern. Large black and white bullseye targets part of AFRC DIC.

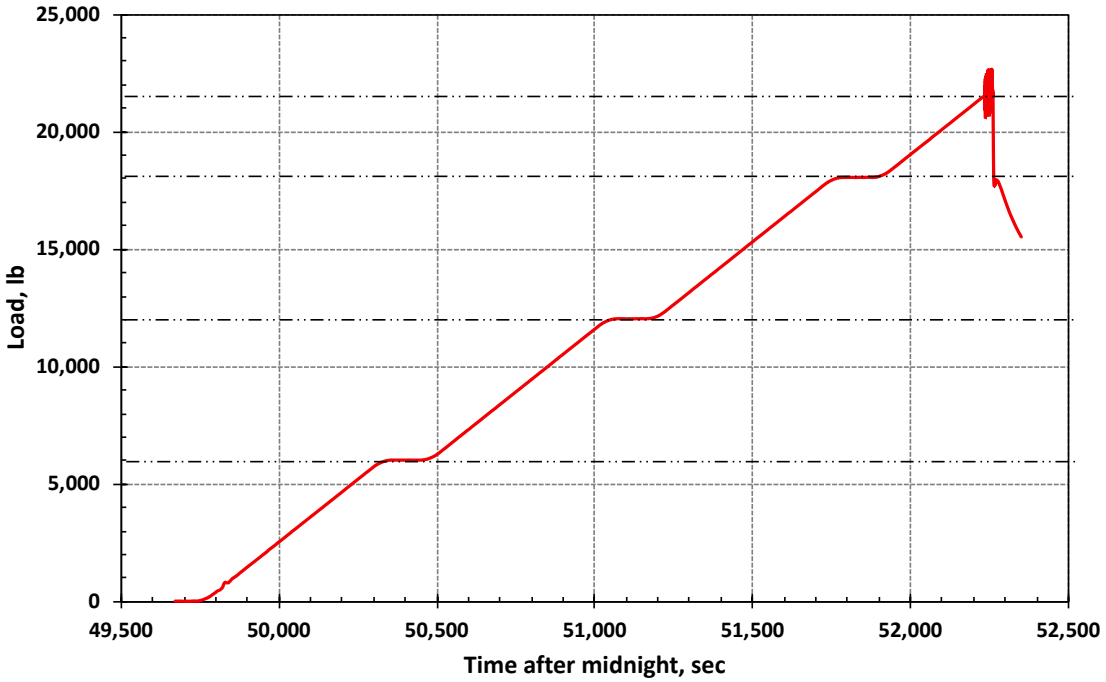

Figure 6. Load versus time plot for the final 2.5g loading.

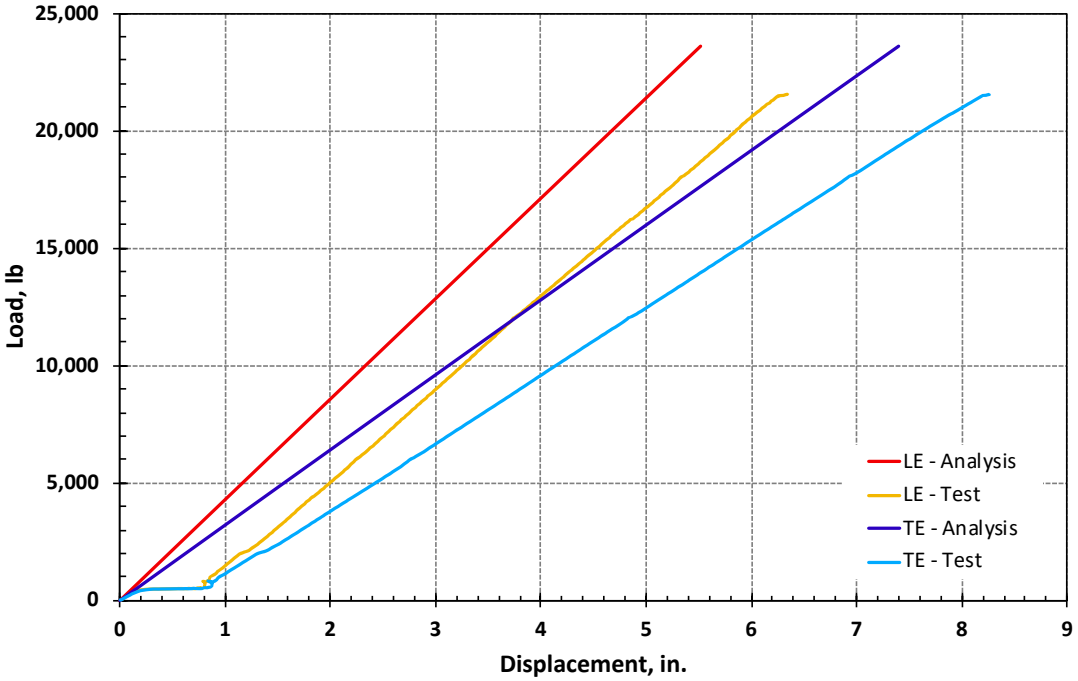

Figure 7. Load versus displacement plot at load line location 2 (approximately 30% span).

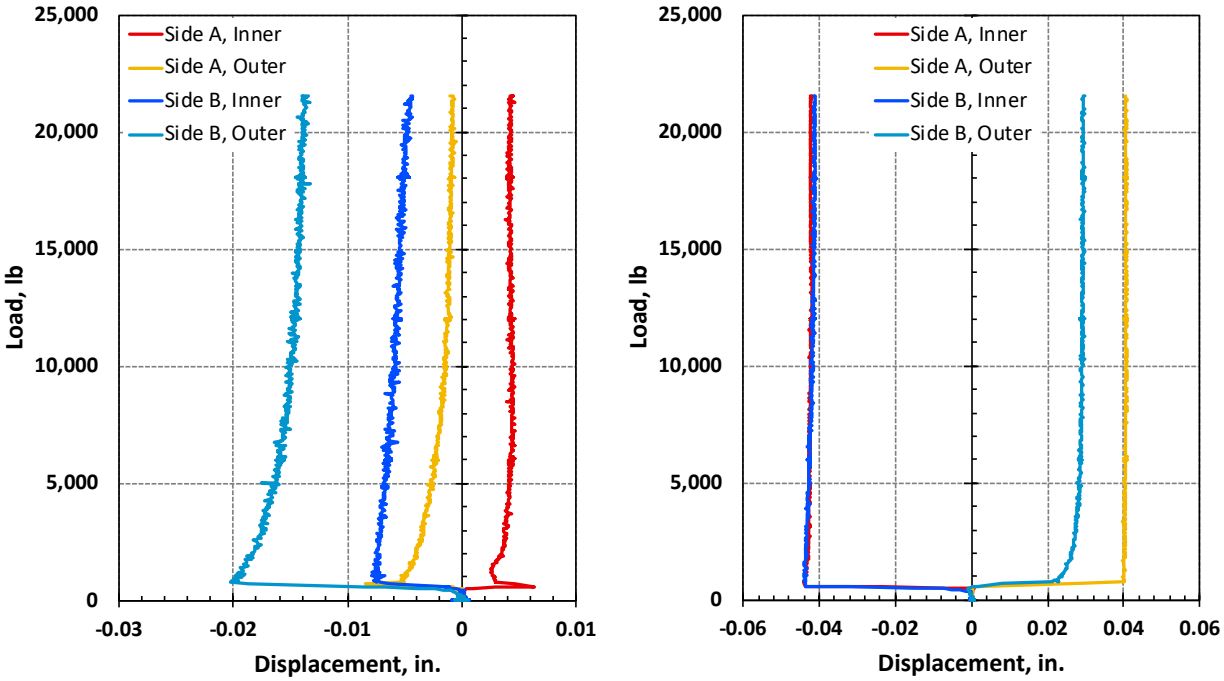

a) Horizontal (outboard positive) b) Vertical (upward positive)

Figure 8. DIC-measured 3-inch attachment pin displacement with respect to the reaction plate.

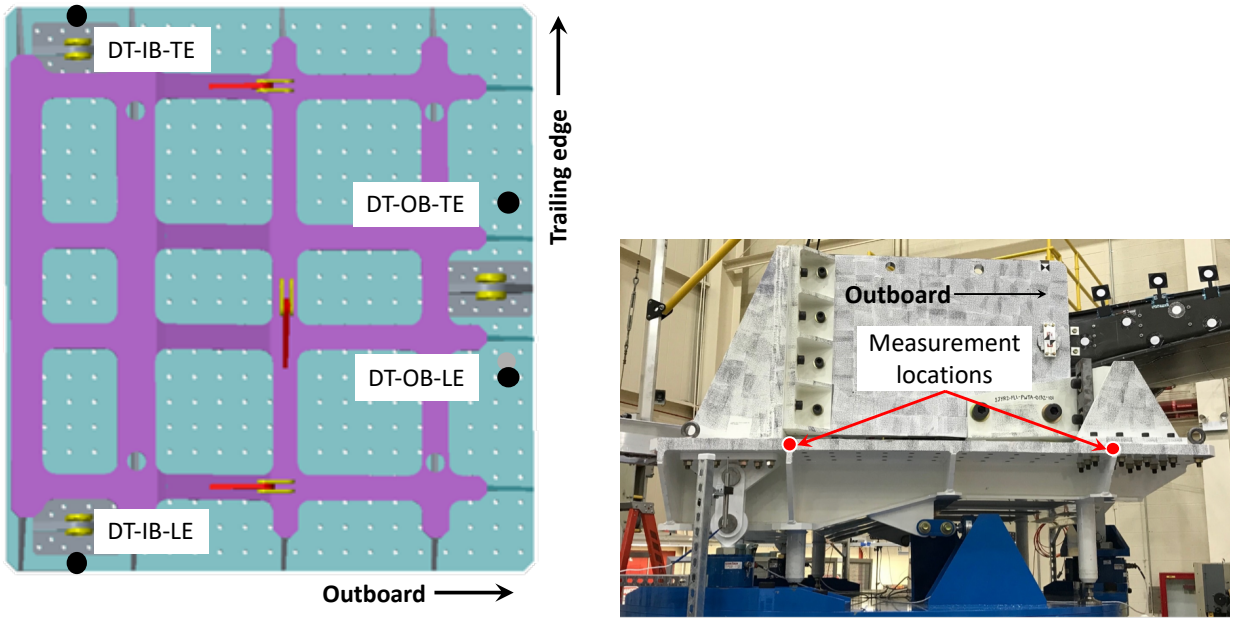

a) DTs (view from bottom) b) DIC (Side A shown, Side B similar)

Figure 9. Reaction table point displacement measurement locations.

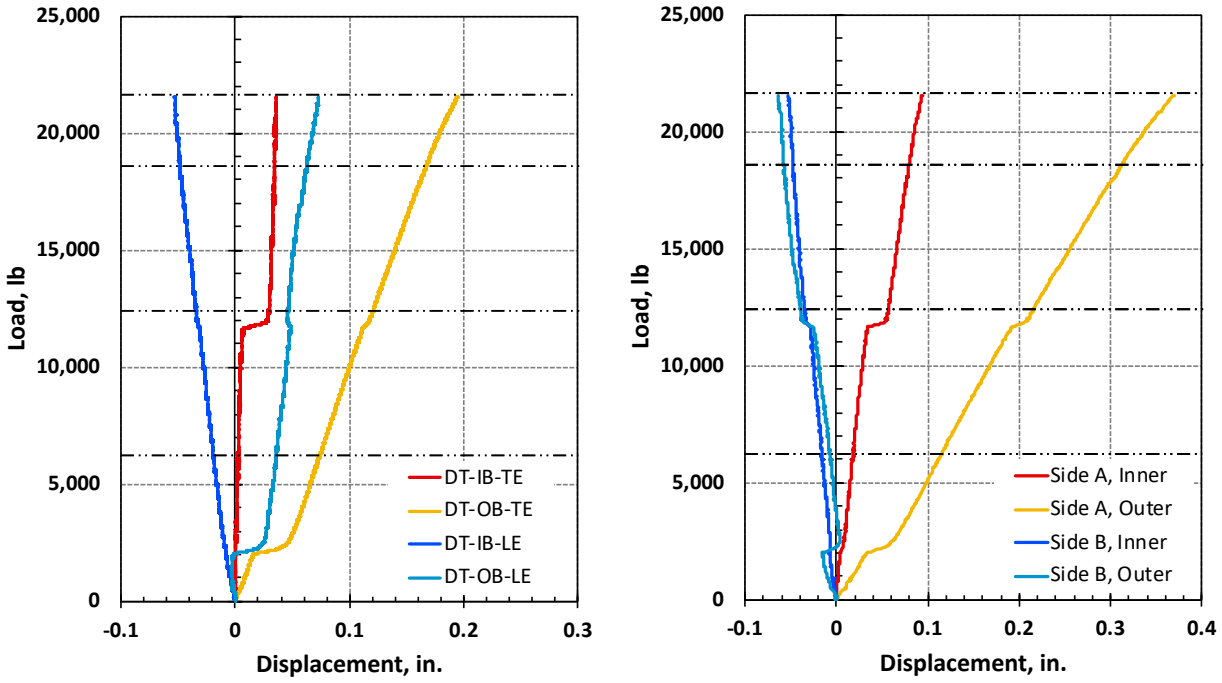

a) DTs b) DIC

Figure 10. Reaction table point vertical displacement measurements at locations identified in Fig. 9.

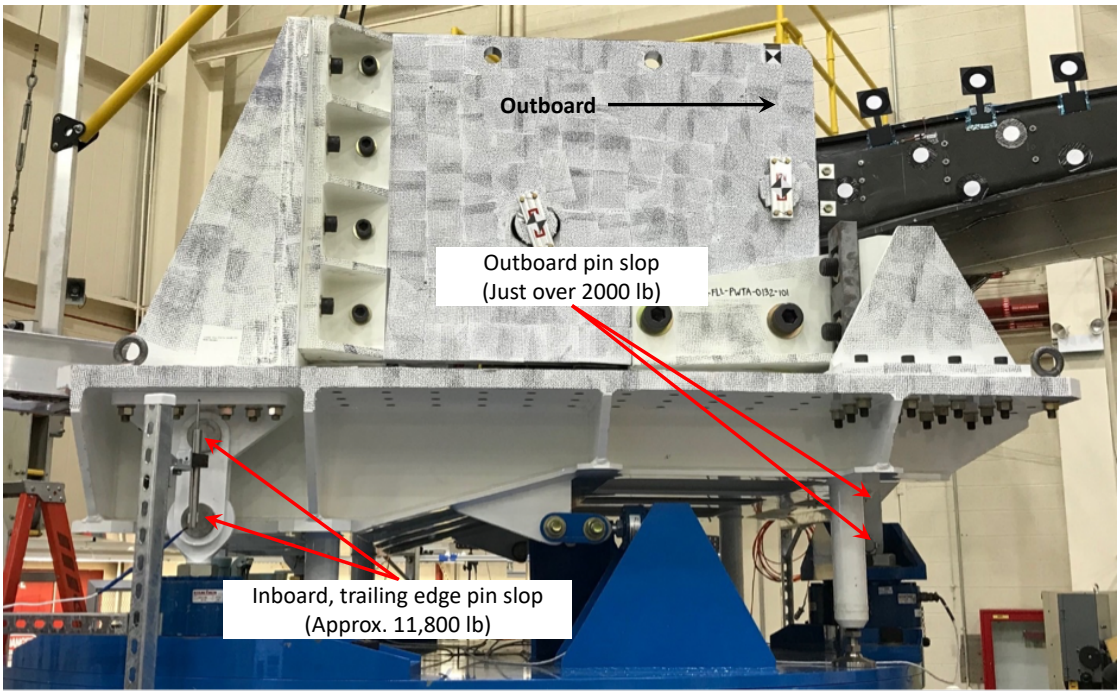

Figure 11. Reaction table load line pin slop locations.

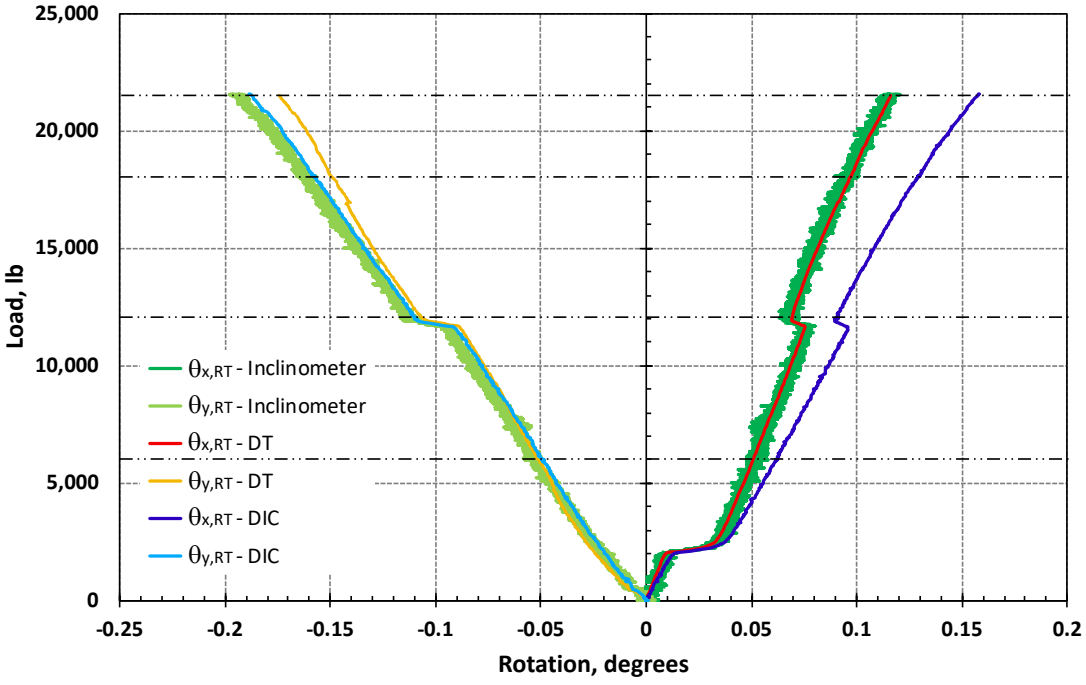

Figure 12. Reaction table load rigid body rotations measured (inclinometer) and calculated (DT, DIC). (Note: Inclinometer values are change in angle from unloaded condition.)

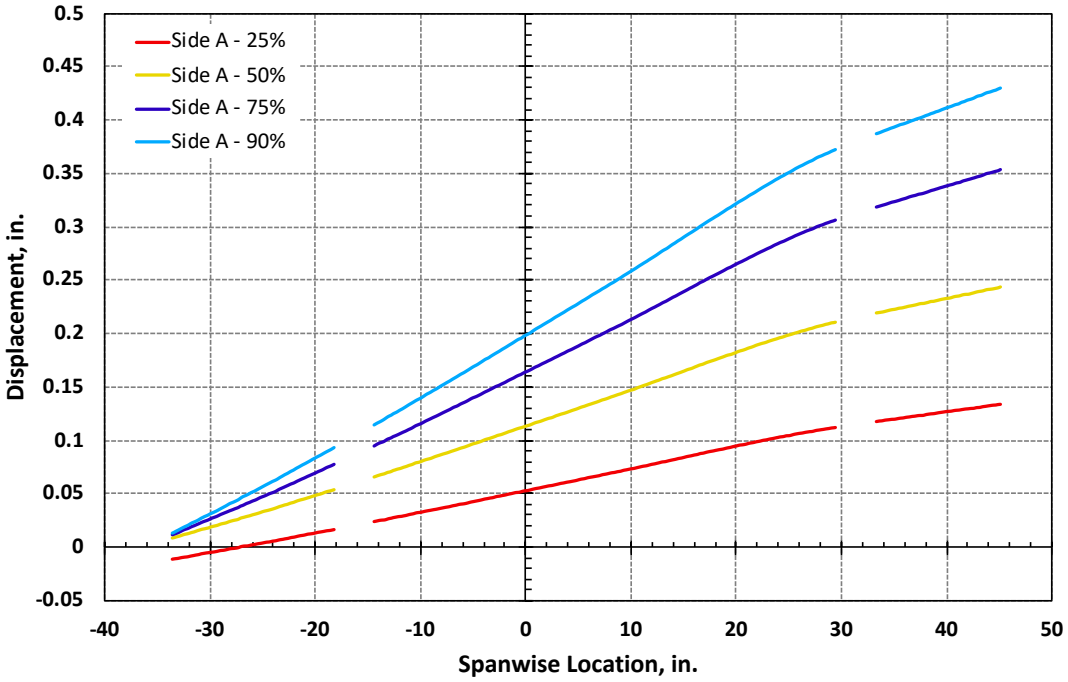

Figure 13. Reaction table edge deformation for trailing edge (Side A).

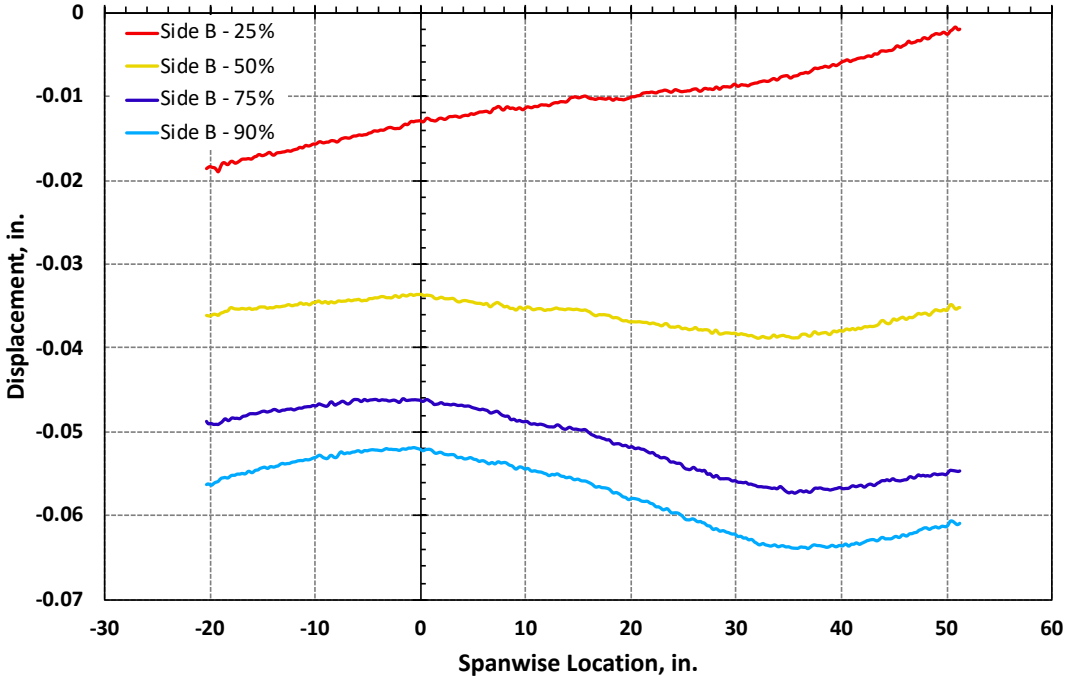

Figure 14. Reaction table edge deformation for leading edge (Side B).

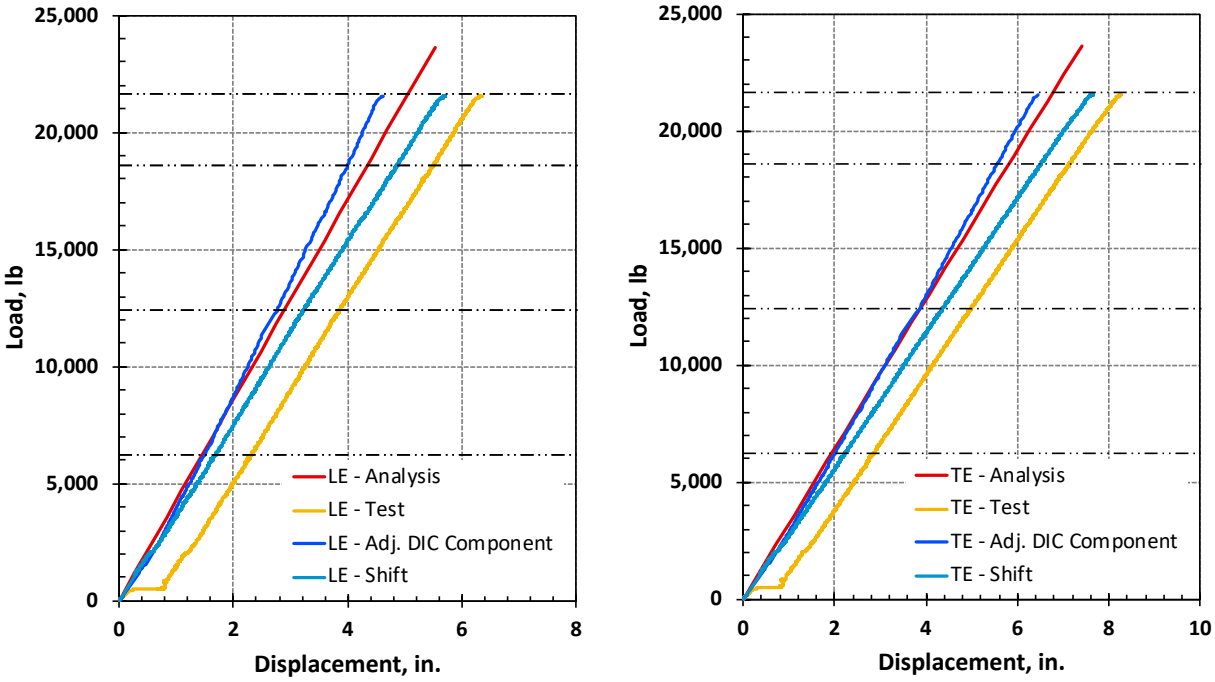

a) Leading edge b) Trailing edge

Figure 15. Load versus displacement comparison at load line location 2 (approximately 30% span).

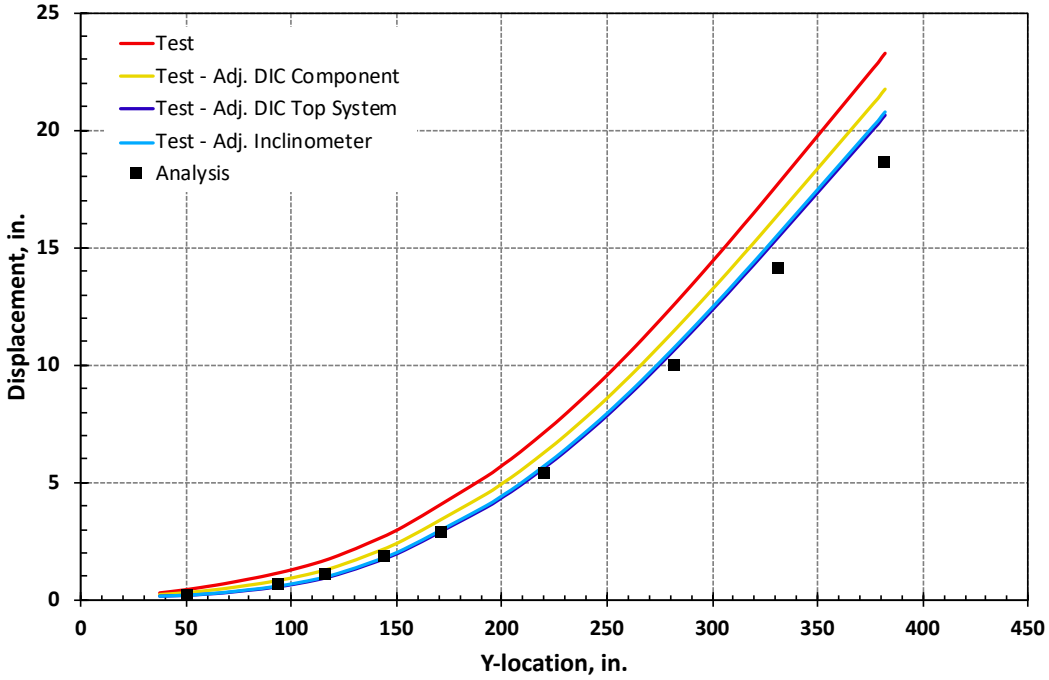

Figure 16. Trailing edge deflection at 25% of 2.5g up-bending load.

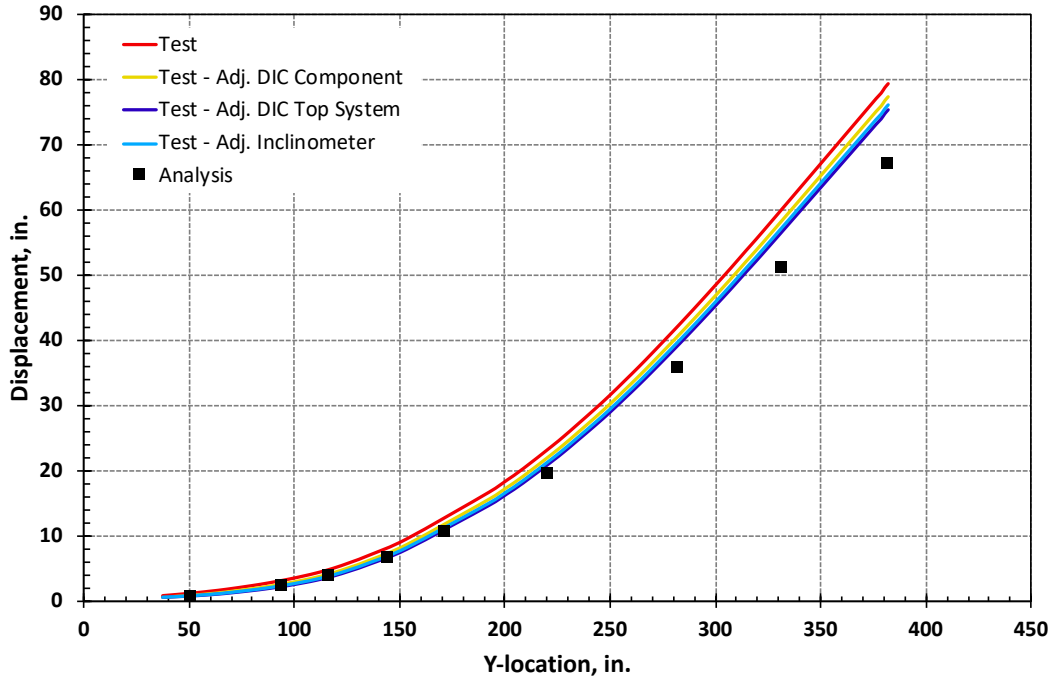

Figure 17. Trailing edge deflection at 90% of 2.5g up-bending load.

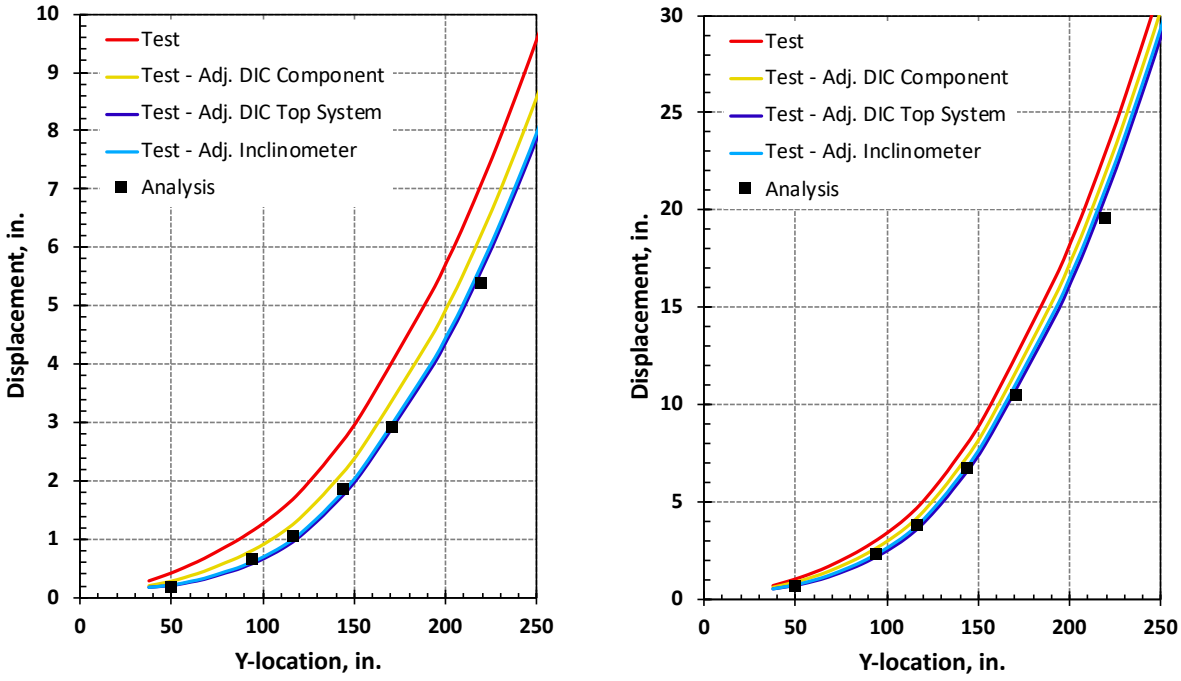

a) 25% load b) 90% load

Figure 18. Inboard trailing edge deflection at 25% and 90% of 2.5g up-bending load.

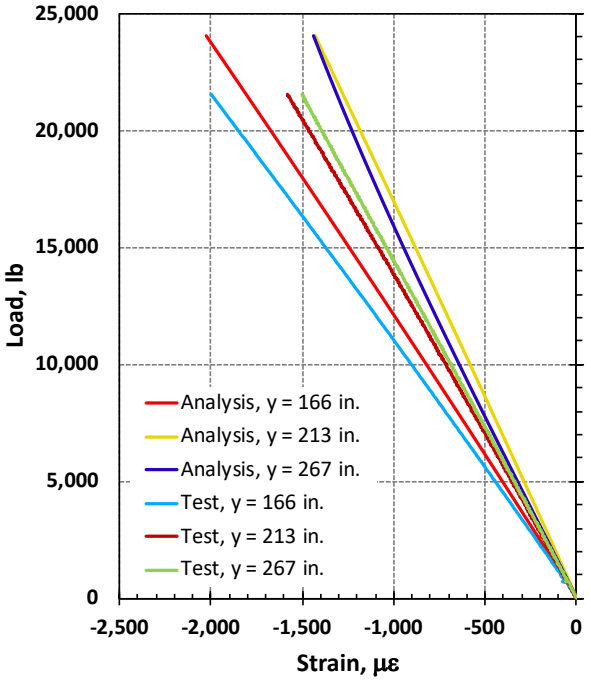

Figure 19. Upper cover axial strain near leading edge.

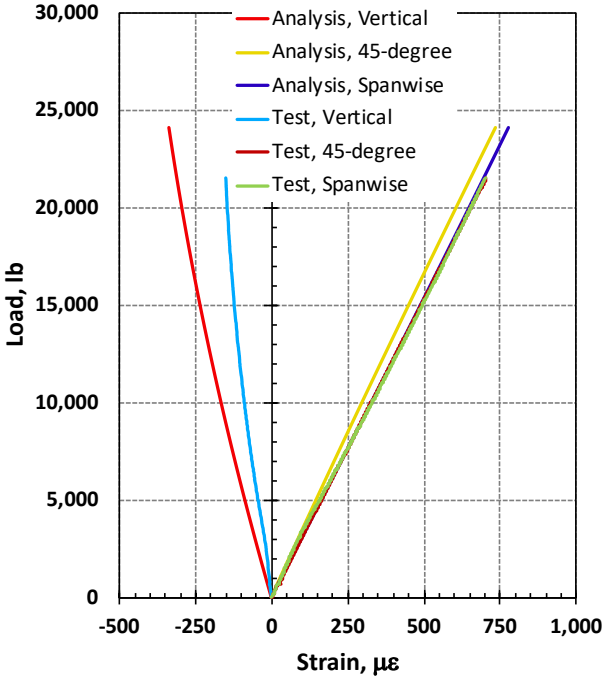

Figure 20. Leading-edge spar rosette strains at 155-inch y-location.

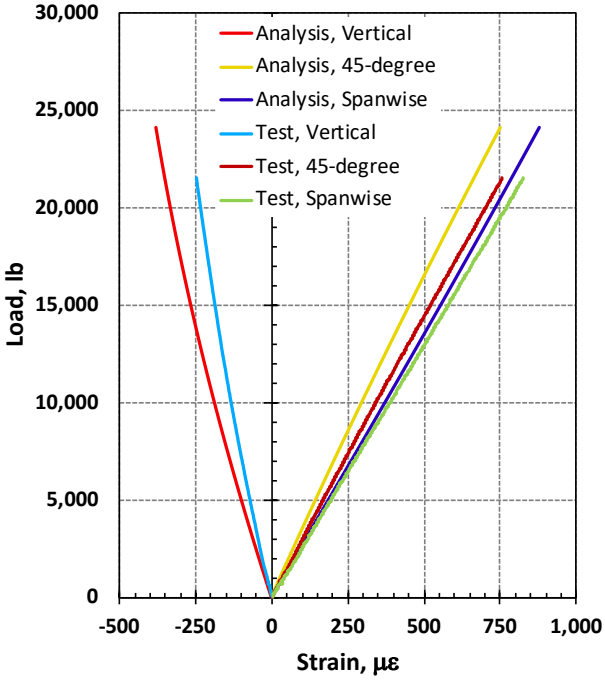

Figure 21. Leading-edge spar rosette strains at 213-inch y-location.

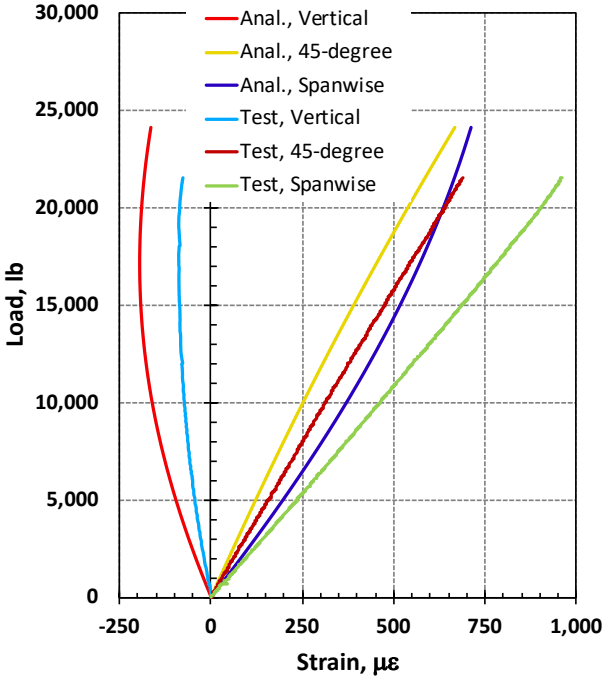

Figure 22. Leading-edge spar rosette strains at 268-inch y-location.